ORIGINAL ARTICLE

lajss.org© Latin American Journal of Solids and Structures

www.lajss.org

Development of train ride comfort prediction model for railway slab track system

Javad Sadeghi[a]* , Siamak Rabiee[a] , Amin Khajehdezfuly[b]

[a]School of Railway Engineering, Iran University of Science and Technology, Narmak, Tehran, Iran; Email: javad_sadeghi@iust.ac.ir, siamak_rabiee@rail.iust.ac.ir

[b]Faculty of Civil Engineering and Architecture, Shahid Chamran University of Ahvaz, Ahvaz, Iran. Email: amin_dezfuly@scu.ac.ir

*Corresponding author

https://doi.org/10.1590/1679-78256237

Abstract

Despite considerable importance of train ride comfort (TRC) in railway slab tracks, there is no TRC prediction model for the slab tracks in the available literature. In this regard, a practical TRC prediction model was developed in this research, taking into account all the track and rolling stock influencing parameters. For this purpose, a vehicle/slab-track interaction model was developed. The model was validated using the results obtained from a comprehensive field test. The effects of rail pad, resilient layer, subgrade, properties of rolling stock suspension systems and vehicle speed on the TRC were studied through a parametric study of the model in which random rail irregularities with various severities were considered. The results obtained were used to develop the TRC prediction model. The accuracy of the model predictions was evaluated by comparing them with those obtained from a railway field. It was shown that the TRC prediction model developed here is a reliable tool for estimation of the TRC from slab track properties, rolling stock parameters and track irregularities. Applicability of the model in the real world of practice is illustrated.

Keywords

Concrete slab track, Ride comfort, Prediction model, Rail irregularity, Vehicle/slab track interaction.

Graphical Abstract

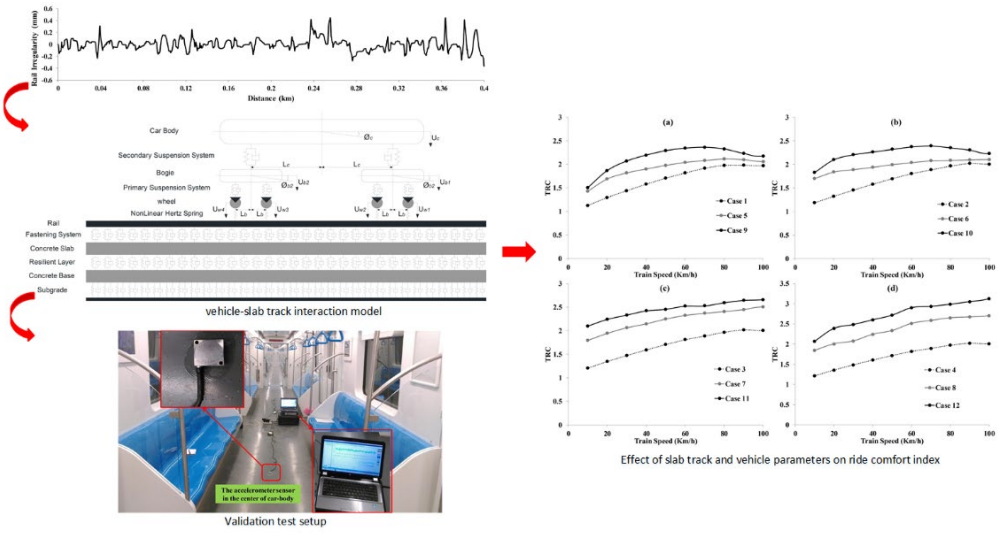

Received: August 18, 2020. In Revised Form: August 21, 2020. Accepted: August 23, 2020. Available online: August 26, 2020.
https://doi.org/10.1590/1679-78256237

1 Introduction

Slab tracks have been widely used in the railway industry because of their less geometry deficiencies compared to other types of railway tracks. However, slab tracks have less capacity in absorption/damping of railway-induced vibration and noise. Train ride comfort (TRC) is one of the most important vibration indicator of railway vehicle performance. It is influenced by properties of train's suspension systems, vehicle speed and railway track conditions including rail irregularities and track condition (Connolly et al. 2015, Kim et al. 2003, Kouroussis et al. 2014, Zakeri et al. 2016).

The TRC is computed based on the standards (see, e.g., BS 6841, 1987; EN 12299, 2009; ISO 2631-1, 1997; UIC 513R, 1994) and Sperling method (Van Eldik Thieme, 1961), presented as a function of carbody accelerations. Carbody accelerations are either measured from the field (Kim et al. 2008, Zhai et al. 2015) or computed from analyses of the results obtained from numerical models of train-track interaction (Choi et al. 2013, Graa et al. 2014, Kargarnovin et al. 2005, Wu and Yang, 2003, Yau et al. 1999). The field measurements require instrumentation of devices and complicated data recoding process which are considerably costly (Kim et al., 2008; Zhai et al., 2015). On the other hand, derivation of accelerations from theoretical models is time consuming interaction (Choi et al. 2013, Graa et al. 2014, Kargarnovin et al. 2005, Wu and Yang, 2003, Yau et al. 1999). The TRC (obtained from measurements or prediction models) is required for making decisions in operation and maintenance of railways. Although, some TRC prediction models have been developed for the ballasted tracks (Sadeghi et al. 2020), no model is available for the slab tracks. Since properties of ballasted tracks are very different from those of slab tracks, there is a need to develop a new TRC prediction model for slab track systems. This need is responded in this research.

The first step in the development of a prediction model is identification of the influencing parameters. Effects of various parameters (such as track condition, properties of vehicle suspension systems, rail irregularities and vehicle speed) on the TRC were investigated in the literature, particularly for the ballasted tracks. For instance, Choi et al. (2013), Kargarnovin et al. (2005), Wu and Yang (2003) and Yau et al. (1999) investigated the effects of rail irregularities and train speeds on response of a train moving over a ballasted railway track. Also, effects of rail irregularities on the TRC were studied by Cheng and Hsu (2014, 2016) and Youcef et al. (2013). Effects of ballasted track flexibility on the acceleration of carboy variation have been investigated in several studies including Cheli and Corradi (2011), Xu et al. (2016) and Kouroussis et al. (2012). In addition to the properties of the track, the Influence of rolling stock (such as vehicle suspension systems parameters) on the TRC have been studied in the literature (Dumitriu 2012, 2013, Dumitriu and Gheţi, 2018, Dumitriu and Stănică 2019).

Investigation of the TRC in railway slab track systems is limited to few works. For instance, Zhai et al. (2009) studied the influence of train speed on the TRC using a two-layered interaction model in which two parallel rails and a concrete slab were considered. Wei et al. (2016) investigated the effect rail pad on the vibration response of car body in a certain speed. The influences of stiffness and damping of rail pad, cement asphalt mortar (CAM) and subgrade on dynamic performance of a vehicle were investigated by Lei (2017) and Zhang et al. (2013). The main limitation of their research is a lack of consideration of rail irregularity, which is mostly observed in the tracks. The importance of the effects of rail irregularities on the TRC has been shown by Sadeghi et al. (2019)

Evaluation of the results obtained in the literature indicates that the main track and rolling stock parameters, which have noticeable influences on the TRC, are vehicle suspension system properties, rail irregularities, vehicle speed and track stiffness. In this research, the previous researches were further developed (extended) by including rail irregularity effects on the TRC. Furthermore, the influencing levels of each parameter on the TRC were quantified. The results were used to develop a comprehensive and practical TRC prediction model for railway slab tracks.

2 Development of vehicle-track model

In order to investigate the effects of track and rolling stock parameters on the TRC, a 2D numerical model of vehicle-slab track dynamic interaction was developed in this study. This model is an upgraded/improved version of the one developed by these authors in (Sadeghi et al. 2016a, 2019). In the new model, the concrete slab is simulated as a continuous layer, which has less computational cost compared to the original one. The model includes the slab-track and the vehicle system. A schematic view of the model is presented in Figure 1.

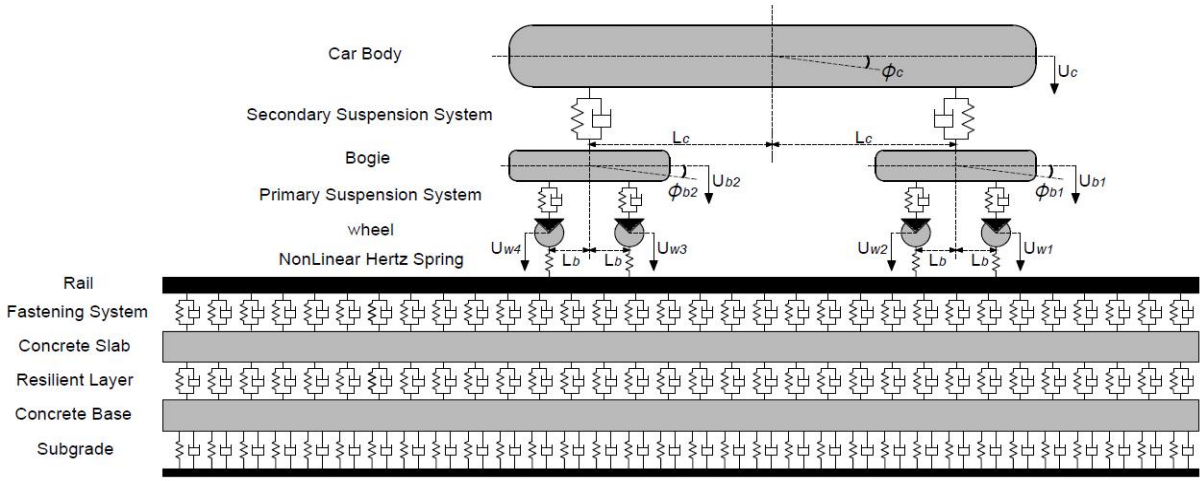

Figure 1 Schematic view of vehicle-slab track interaction model

The slab track sub-model consists of the rail, concrete slab and concrete base, which are simulated as a continuous layer using the Euler-Bernouli beam element. The beam element has four Degrees Of Freedom (DOF), with cubic Hermitian shape functions. The mass and stiffness matrices ($[M]_{beam}$ and $[K]_{beam}$) of the beam element can be defined as follows: (Mosayebi et al. 2020)

$$[K]_{beam} = \frac{EI}{l^3}\begin{bmatrix} 12 & 6l & -12 & 6l \\ 6l & 4l^2 & -6l & 2l^2 \\ -12 & -6l & 12 & -6l \\ 6l & 2l^2 & -6l & 4l^2 \end{bmatrix} \qquad [M]_{beam} = \frac{ml}{420}\begin{bmatrix} 156 & 22l & 54 & -13l \\ 22l & 4l^2 & 13l & -3l^2 \\ 54 & 13l & 156 & -22l \\ -13l & -3l^2 & -22l & 4l^2 \end{bmatrix} \tag{1}$$

where *m*, *EI* and *l* represent the mass per unit length, the flexural rigidity and the length of the beam element, respectively. As shown in Figure 1, fastening system connects the rail layer to the concrete slab layer. The concrete slab layer was attached to the concrete base layer using a resilient layer. The concrete base layer was laid on a subgrade. The fastening system (rail pad), resilient layer and subgrade are simulated as linear spring–dashpot elements. By assembling the elements, the slab track matrices of mass ($[M_T]$), damping ($[C_T]$) and stiffness ($[K_T]$) were derived. The governing differential equation of the motion was provided in Khajehdezfuly (2019). The vehicle was simulated as a wagon with ten DOFs (Mosayebi et al. 2017). The car body has a mass of M_C and a rotational moment of J_C about the transverse axis. Similarly, each bogie frame has a mass of M_b and rotational moment of J_b. Each wheel was characterized by a mass of M_w. The mass matrix ($[M_V]$), the damping matrix ($[C_V]$) and the stiffness matrix ($[K_V]$) of vehicle were defined by equations (2) to (4), respectively (Askarinejad and Dhanasekar 2016, Khajehdezfuly 2019, Mosayebi et al. 2017, Sadeghi et al. 2016b, 2019)

$$[M_V] = diag[M_C \quad J_C \quad M_b \quad J_b \quad M_b \quad J_b \quad M_w \quad M_w \quad M_w \quad M_w] \tag{2}$$

$$[C_V] = \begin{bmatrix} 2C_b & 0 & -C_b & 0 & -C_b & 0 & 0 & 0 & 0 & 0 \\ 0 & 2C_bL_c^2 & -C_bL_c & 0 & -C_bL_c & 0 & 0 & 0 & 0 & 0 \\ -C_b & -C_bL_c & C_b+2C_w & 0 & 0 & 0 & -C_w & -C_w & 0 & 0 \\ 0 & 0 & 0 & 2C_wL_b^2 & 0 & 0 & -C_wL_b & -C_wL_b & 0 & 0 \\ -C_b & -C_bL_c & 0 & 0 & C_b+2C_w & 0 & 0 & 0 & -C_w & -C_w \\ 0 & 0 & 0 & 0 & 0 & 2C_wL_b^2 & 0 & 0 & -C_wL_b & -C_wL_b \\ 0 & 0 & -C_w & -C_wL_b & 0 & 0 & C_w & 0 & 0 & 0 \\ 0 & 0 & -C_w & -C_wL_b & 0 & 0 & 0 & C_w & 0 & 0 \\ 0 & 0 & 0 & 0 & -C_w & -C_wL_b & 0 & 0 & C_w & 0 \\ 0 & 0 & 0 & 0 & -C_w & -C_wL_b & 0 & 0 & 0 & C_w \end{bmatrix} \tag{3}$$

$$[K_V]=\begin{bmatrix} 2K_b & 0 & -K_b & 0 & -K_b & 0 & 0 & 0 & 0 & 0 \\ 0 & 2K_bL_c^2 & -K_bL_c & 0 & -K_bL_c & 0 & 0 & 0 & 0 & 0 \\ -K_b & -K_bL_c & K_b+2K_w & 0 & 0 & 0 & -K_w & -K_w & 0 & 0 \\ 0 & 0 & 0 & 2K_wL_b^2 & 0 & 0 & -K_wL_b & -K_wL_b & 0 & 0 \\ -K_b & -K_bL_c & 0 & 0 & K_b+2K_w & 0 & 0 & 0 & -K_w & -K_w \\ 0 & 0 & 0 & 0 & 0 & 2K_wL_b^2 & 0 & 0 & -K_wL_b & -K_wL_b \\ 0 & 0 & -K_w & -K_wL_b & 0 & 0 & K_w & 0 & 0 & 0 \\ 0 & 0 & -K_w & -K_wL_b & 0 & 0 & 0 & K_w & 0 & 0 \\ 0 & 0 & 0 & 0 & -K_w & -K_wL_b & 0 & 0 & K_w & 0 \\ 0 & 0 & 0 & 0 & -K_w & -K_wL_b & 0 & 0 & 0 & K_w \end{bmatrix} \quad (4)$$

Finally, the governing differential equation of motion for the vehicle was derived as described in Costa et al. (2012, 2015) and Fernández Ruiz et al. (2017). The vehicle acceleration vector was obtained by the second derivative of the vehicle displacement as under:

$$\{\ddot{d}_V\}=\{\ddot{U}_C \quad \ddot{\Phi}_C \quad \ddot{U}_{b1} \quad \ddot{\Phi}_{b1} \quad \ddot{U}_{b2} \quad \ddot{\Phi}_{b2} \quad \ddot{U}_{w1} \quad \ddot{U}_{w2} \quad \ddot{U}_{w3} \quad \ddot{U}_{w4}\}^T \quad (5)$$

where $\ddot{U}_C$ is the carbody vertical acceleration. The non-linear Hertz contact theory was implemented for simulation of the interaction between wheel and rail. The contact force between the rail and the wheel is obtained as follows: (Sun and Dhanasekar 2002, Zhang et al. 2012)

$$F_H=\begin{cases} C_H(U_{wheel}-U_{Rail}-U_{Irr})^{\frac{3}{2}} & U_{wheel}-U_{Rail}-U_{Irr}>0 \\ 0 & U_{wheel}-U_{Rail}-U_{Irr}\le 0 \end{cases} \quad (6)$$

where F_H is the contact force between the wheel and the rail, U_{wheel} stands for the wheel vertical displacement, U_{Rail} is the rail vertical displacement of the wheel-rail contact point, U_{Irr} stands for the rail irregularity and C_H is the Hertz spring constant. The stiffness, mass and damping matrices of the whole model were derived by assembling the stiffness, mass and damping matrices of the sub-models (Askarinejad and Dhanasekar 2016, Khajehdezfuly 2019, Sadeghi et al. 2016a, 2016b, Sadeghi et al. 2019). The vehicle-slab track dynamic interaction equation was solved using Advanced Solution Algorithm (ASA) developed by Sadeghi et al. (2016a). The total acceleration vector was obtained from equation (5) and subsequently the time history of the carbody vertical acceleration ($\ddot{U}_C(t)$) was derived in the time domain. This study is limited to the straight lines (i.e., no curves considered). It means that there is no lateral interaction between the vehicle and the track. Therefore, only the vertical vibration of the vehicle was considered (Sadeghi et al. 2019).

The Sperling index (W_Z) was used to represent the level of the TRC. The Sperling index has been suggested as an appropriate criterion for the TRC because of its simplicity and accuracy (Esveld 1989, Iwnicki 2006, Kargarnovin et al. 2005, Ketchum and Wilson 2012, Kumar et al. 2017, Ling et al. 2018, Yang et al. 2004). For the computation of the Sperling index, there is not any limitation for the time duration of data sampling. Therefore, it has low computational cost. Other ride comfort indexes such as EN or UIC need at least five minutes of accelerations time history, which cause substantially higher computational cost. Moreover, the Sperling index requires the least instrumentations for the field measurements (i.e., it needs only biaxial accelerometers). These reasons indicate the suitability of the Sperling index for the prediction of the TRC (Sadeghi et al. 2019). The vertical acceleration of carbody ($\ddot{U}_C(t)$) obtained from the vehicle/track interaction model was transferred into the frequency domain using the Fast Fourier Transformation (FFT). The vehicle response was weighted by the Sperling's filter (B(f)) in the frequency domain (Esveld 1989, Kumar et al. 2017). The Sperling frequency weighting filter (B(f)) is drawn in Figure 2. Finally, the comfort index (W_Z) was obtained using the Root Mean Square (RMS) of the weighted accelerations as follows: (Esveld 1989, Kumar et al. 2017)

$$W_Z=4.42\left(\sqrt{\frac{1}{n}\sum_{i=1}^{n}a_{wi}^2}\right)^{0.3} \quad (7)$$

where a_{wi} is the weighted acceleration (by the Sperling's filter) in the time domain. Definitions of different levels of Sperling index are presented in Kumar et al. (2017). For instance, the W_Z shall be less than 2.5 to have moderate comfortable condition.

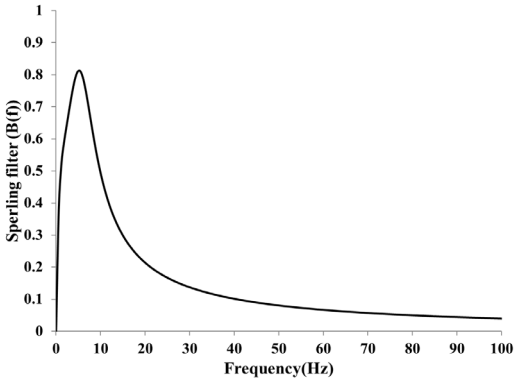

Figure 2 Sperling frequency weighting filter (B(*f*))

3 Validation of vehicle-track model

Validity of the model was examined through comparison between the results obtained from the model and those of a comprehensive field measurement carried out in this research. The test procedure and comparisons of the results are discussed in the following sections.

3.1 Field test

The field test was carried out in Line 1 of Isfahan's metro (the second largest subway network in Iran). The location of the test was between Takhti and Imam Hossein stations (Figure 3). A polyurethane resilient layer exists between concrete slab and the tunnel lining which forms a Floating Slab Track (FST) (Figure 4). The properties of the slab track are presented in Table 1. The tested track had a length of 0.4 km (Km 12+329 to 12+729). It was divided into 10 segments. The rail irregularities at the test locations were measured by a trolley system. The rail irregularity profiles measured for the track are presented in Figure 5. The Chinese train type of Pouzhen was used in the field test. Characteristics of the train used in the field test are presented in Table 2. A view of the train used is shown in Figure 6. One accelerometer with the capacity of 1 g was installed on the floor at the center of the wagon to measure the vertical accelerations of the car body in all the tests (Figure 7). The tests were performed with the train speeds of 30 and 50 km/h. The ECON data logger was used to record the data (Figure 7) and a sampling frequency was 640 Hz. A sample of recorded accelerations is presented in Figure 8.

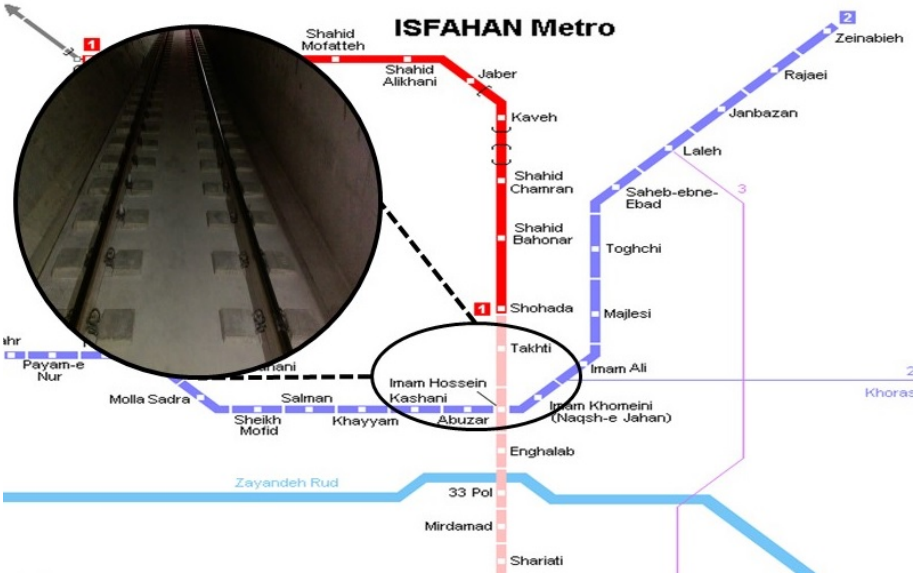

Figure 3 Field test location in Isfahan metro line 1 between Takhti and Imam Hossein stations

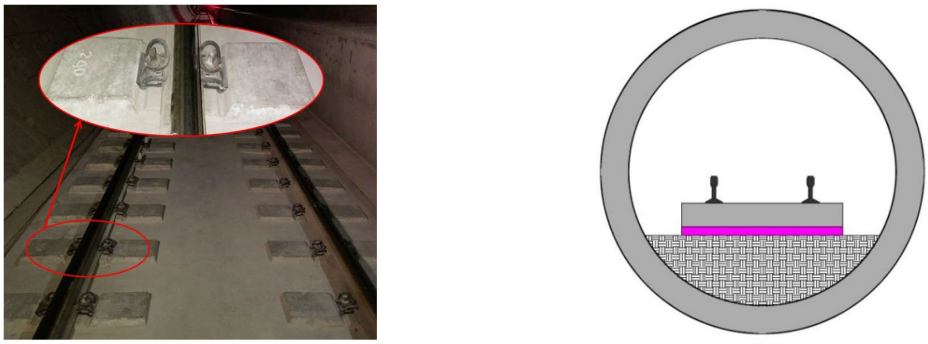

(a) (b)

Figure 4 Views of the superstructure of slab track in the field test: (a) View of slab track; (b) schematic view Floating Slab Track (FST).

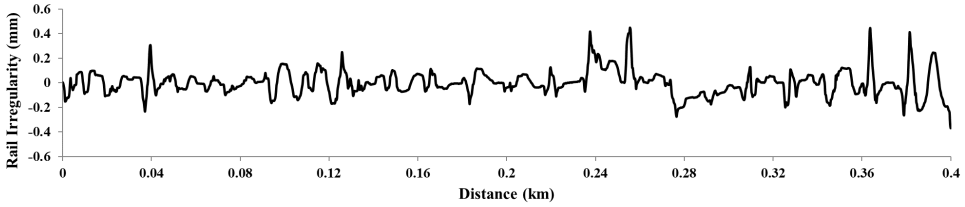

Figure 5 Rail irregularity of field test location in Isfahan's metro

(a) (b)

Figure 6 Views of the vehicle in the field test: (a) View from outside of Isfahan metro vehicle; (b) View from inside of Isfahan metro vehicle

Table 1 Slab-track properties (adapted from IMER Co 2005 and Sadeghi et al., 2016b).

Component	Properties	Magnitude
Rail S49	Flexural rigidity	3819900 $N.m^2$
	Mass per unit length	49.69 kg/m
Fastening system	Fastening space	0.6 m
	Rail pad stiffness	15×10^7 N/m
	Rail pad damping	3×10^4 $N.s/m$
Concrete slab	Length	11.37 m
	Width	2.6 m
	Thickness	0.4 m
	Elastic modulus	35 GPa
	Density	2500 kg/m^3
Polyurethane sylomer SR 18	Thickness	0.025 m
	Dynamic modulus	28×10^4 N/m^2
	Stiffness	11648000 N/m^3
	Damping	243549 $N.s/m^3$
Concrete base	Width	2.6 m
	Thickness	0.3 m
	Elastic modulus	33 GPa
	Density	2500 kg/m^3
Subgrade	Stiffness	13.1×10^7 N/m^2
	Damping	7.7×10^4 $N.s/m^2$

Table 2 Characteristics of vehicle in Isfahan field test (adapted from CNR CR, 2014).

Parameters	Value	Unit
Carbody mass	21400	kg
Bogie mass	7500	kg
Wheelset + gear box mass	2000	kg
Primary suspension stiffness	970	kN/m
Secondary suspension stiffness	275	kN/m
Axle load	14	Ton
Wheel base	2.2	m

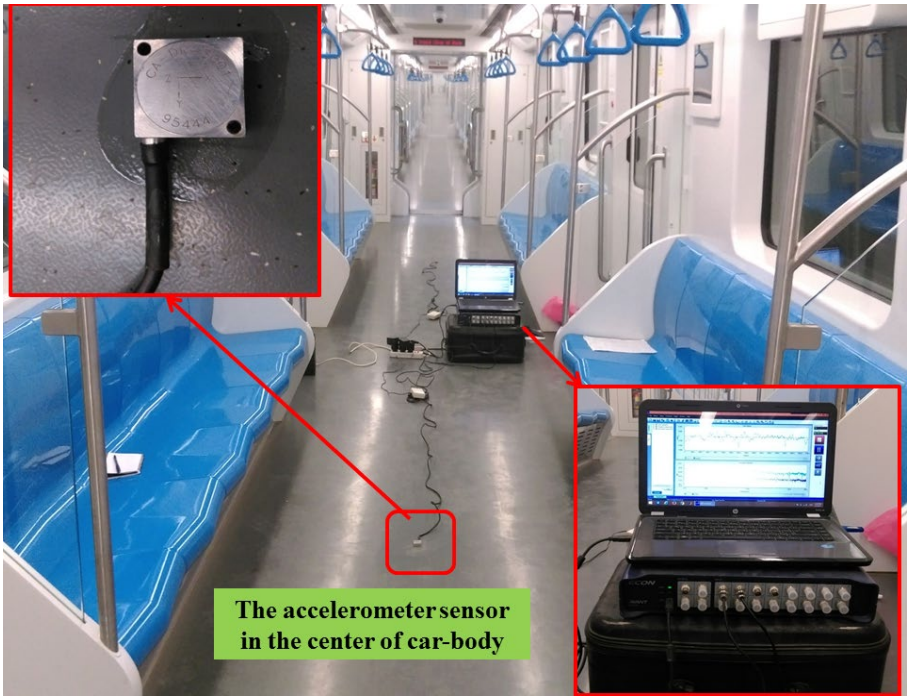

Figure 7 Test setup

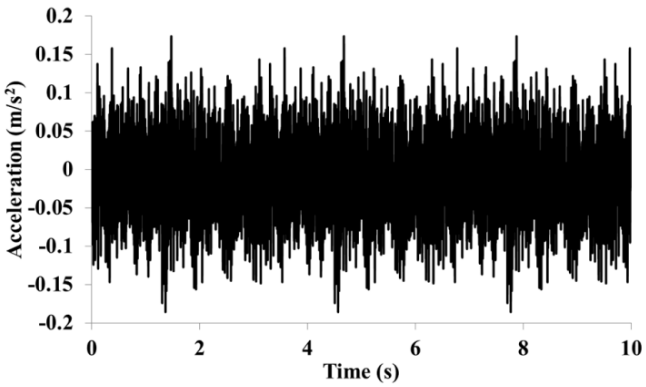

Figure 8 Sample of recorded accelerations with train speed of 30 km/h.

3.2 Comparison of results

Comparisons of the results obtained from the model and the field test for the vehicle speeds of 30 and 50 km/h are presented in Figure 9. According to Figure 9, the differences between the field test results and those of the model are in the range of (2-10%). As presented in Figures 9(a) and 9(b), the maximum difference between W_Z obtained from the model and the experiments is about 10% in the 7th segment when the train speed is 50 km/h. As shown in Figure 5, the severity and amplitude of the rail irregularity in Segment 7 is greater than those of the other segments. The minimum difference (about 2%) between the results is in the 2th segment. Comparisons of the results presented in Figures 9 indicate that the model has a good level of accuracy in prediction of the TRC.

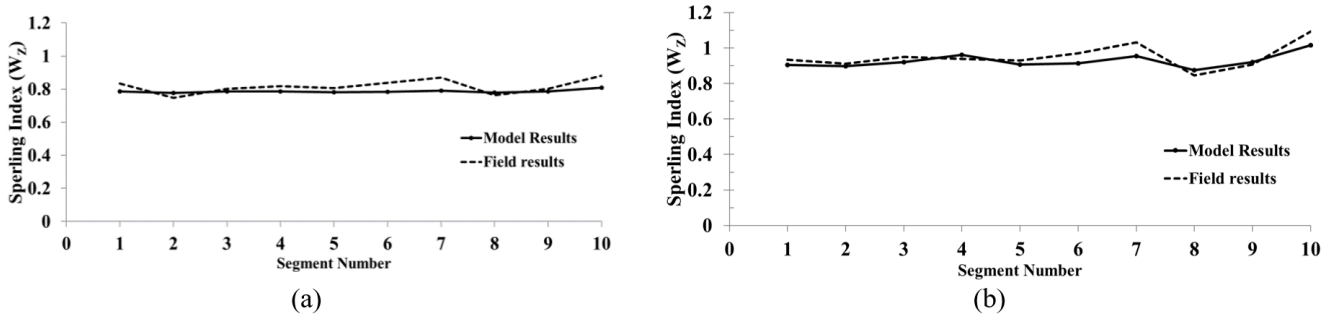

Figure 9 Comparisons of the results obtained from the model and those of the Isfahan field with FST superstructure for two train speeds: (a) 30 km/h; (b) 50 km/h.

4 Effects of track and rolling stock parameters on TRC

According to the literature (discussed above), vehicle suspension system properties, vehicle speed, rail irregularities and track flexibility (stiffness of rail pad, resilient layer and subgrade) are known as the parameters having noticeable effects on the TRC. The model developed and validated above was used to investigate and quantify the effects of these parameters on the TRC.

4.1 Effects of track parameters on the TRC

As presented in Table 3, three types of rail pad, four different resilient layers and three types of subgrade were considered in the investigation. Altogether, 12 types (cases) of slab tracks with various combinations of rail pads and resilient layers were considered (Table 4). They cover the possible conditions of track properties (Khajehdezfuly 2019, Lei and Wang, 2014, Lei and Zhang 2010, Sadeghi and Esmaeili, 2018). The vehicle characteristics were adopted from Chinese railway vehicle called CHR3 (Lei and Wang 2014, Lei and Zhang 2010, Sadeghi et al. 2016b). The vehicle speed was changed from 10 to 100 km/h. The effects of track flexibility and vehicle speed on the TRC were evaluated in presence of random irregularities with low, medium and high severities. The characteristics of rail irregularities were adapted from the Federal Railroad Administration (FRA) classifications (Garg and Dukkipati 1984, Lei 2017, Zakeri et al. 2017)

Table 3 The different levels of slab track components stiffness (MN/m)

Parameters	Case	Value
Rail pad	Soft	15
	Medium	150
	Hard	500
Resilient layer (between slab and concrete base)	Polyurethane-Soft (PU-Soft)	5
	Polyurethane-Hard (PU-Hard)	200
	Cement Asphalt Mortar-Soft (CAM-Soft)	900
	Cement Asphalt Mortar-Hard (CAM-Hard)	5000
Subgrade	Soft	20
	Medium	60
	Hard	120

Table 4 Different cases of combination of rail pads with resilient layers.

Rail pad	Resilient layer			
	PU-Soft	PU-Hard	CAM-Soft	CAM-Hard
Soft	Case 1	Case 2	Case 3	Case 4
Medium	Case 5	Case 6	Case 7	Case 8
Hard	Case 9	Case 10	Case 11	Case 12

The random track vertical irregularities are generated by the power spectral density function (PSD). $S_v(\omega)$ is the mathematical expression of the PSD function presented by the FRA as under: (Garg and Dukkipati 1984, Lei 2017, Zakeri et al. 2017)

$$S_v(\omega) = \frac{A_v\omega_2^2(\omega^2+\omega_1^2)}{\omega^4(\omega^2+\omega_2^2)} \qquad m^2/rad/m \tag{8}$$

where ω (rad/m) is the spatial frequency or wave number, ω_1 and ω_2 are the cutoff frequencies, and A_v is the roughness amplitude. The values of parameters used in equation (8) are addressed in Garg and Dukkipati (1984) and Lei (2017). The random irregularities are generated in three cases for class 4, 5 and 6 (high, medium and low severities, respectively) based on the FRA. The low severity irregularity (class 6) refers to a newly constructed track. The amplitudes of low, medium and high severities irregularity are limited to 2, 5 and 9 mm, respectively (Garg and Dukkipati 1984, Kargarnovin et al. 2005, Lei 2017, Yang et al. 2004). The function of rail irregularity (r(x)) can be generated numerically using the following trigonometric series: (Au et al. 2002)

$$r(x) = 2\sum_{n=1}^{N}\sqrt{S_v(\omega_n)\Delta\omega}\cos(\omega_n x + \theta_n) \qquad n = 1,2,3,\ldots,N \tag{9}$$

where ω_n is the discrete frequency of the PSD function within the interval $[\omega_{min}, \omega_{max}]$, θ_n stands for the random phase angle with a uniform probability distribution in the interval [0,2π], *x* is the global coordinate and *N* is the total number of frequency increments. The parameter ω_n is computed as follows: (Au et al. 2002)

$$\omega_n = \omega_{min} + (n-0.5)\Delta\omega \qquad n = 1,2,3,\ldots,N \tag{10}$$

$$\Delta\omega = \frac{\omega_{max}-\omega_{min}}{N},\ \omega_{max} = \frac{2\pi}{\lambda_{min}} \text{ and } \omega_{min} = \frac{2\pi}{\lambda_{max}} \tag{11}$$

in which ω_{max} and ω_{min} are the upper and lower limits of the frequency ω, Δω stands for the frequency increment, λ_{min} and λ_{max} are the lower and upper limits of wavelength range in which the PSD function is included. The wavelength was considered in the range of 0.5 to 40 m. In addition, 2500 frequency points were used to generate a random irregularity. The typical generated rail irregularities used in the parametric study are presented in Figure 10.

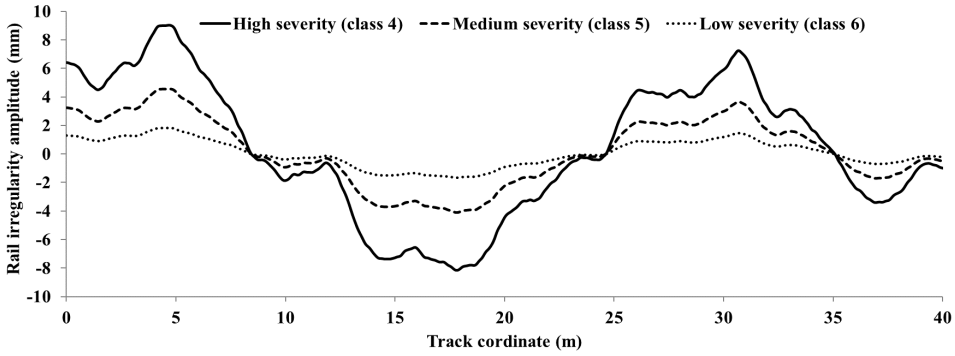

Figure 10 A sample of random irregularities.

Random irregularity with high severity

The results obtained from the analyses of the model in presence of the random irregularity with high severity are presented in Figures 11 and 12. The variations of TRC against the train speed for various stiffness of rail pad, resilient layer (between slab and concrete base) and subgrade are illustrated in these figures. The results indicate that the slab track components flexibility changes the level of TRC (up to 70 percent). Comparison of the results indicates that variation of the TRC against train speed has dissimilar trends for different track flexibilities. In other words, the train speed changes the pattern of track flexibility effect on the TRC. Although subgrade stiffness has no significant influence on the TRC (less than 2 percent), rail pad stiffness and resilient layer stiffness have noticeable influence.

Based on the results presented in Figure 11, rail pad type is an important factor in the trend of TRC variation against train speed. It is observed from Figure 11(a) that when the rail pad is soft, neither resilient layer softness nor subgrade stiffness changes the level of TRC. However, as the rail pad stiffness increases to medium and hard, the influence of resilient layer stiffness on the TRC is increased. For instance, when the rail pad is medium and hard (for the train speed of 100 km/h) there is 28% and 42% changes in the TRC, respectively.

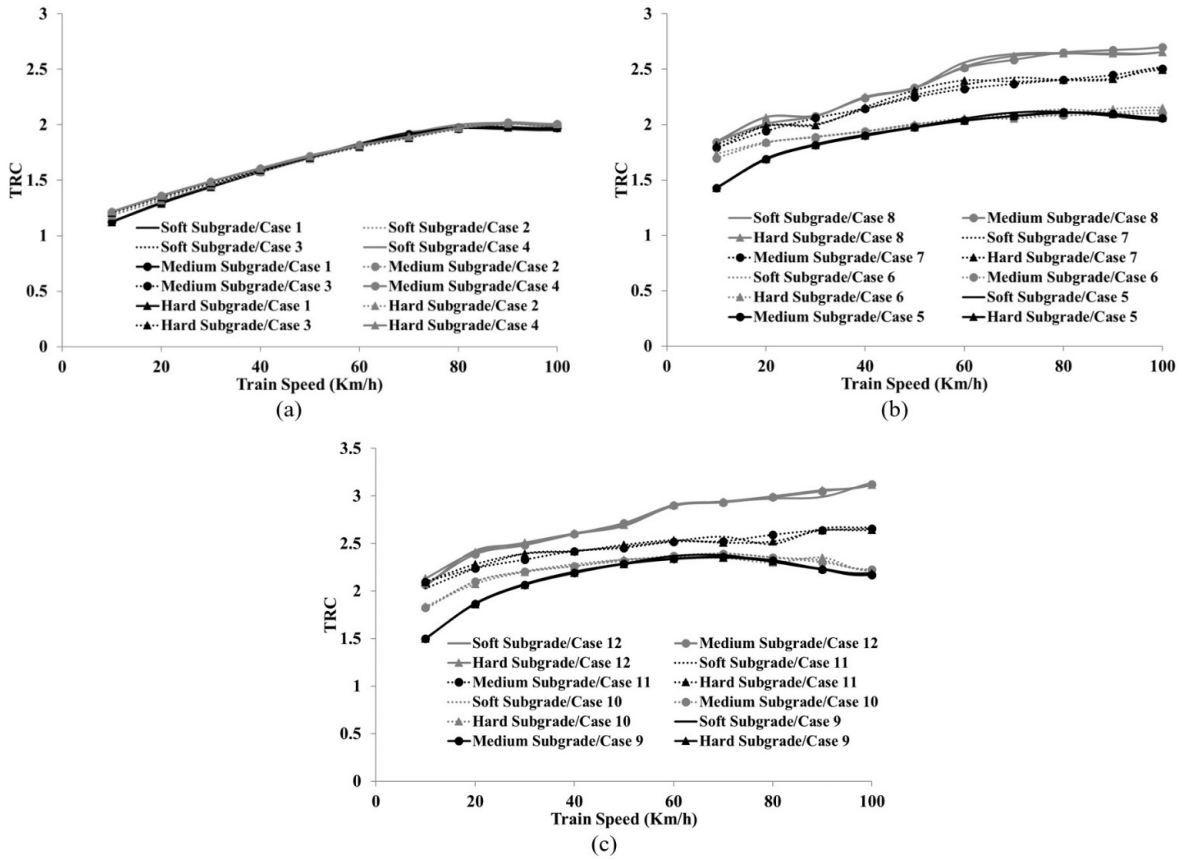

Figure 11 Variations of TRC versus train speed for random irregularities with high severity in various rail pads: (a) Soft rail pad; (b) Medium rail pad; (c) Hard rail pad.

Figures 12(a) to 12(d) illustrate the variation of the TRC against the train speed in various stiffness of resilient layer. It is observed from Figures 12(a) and 12(b) that TRC is significantly influenced by resilient layer stiffness. Based on these figures, the TRC variation is dependent on train speed when there is a PU layer between slab and concrete base (resilient layer with low stiffness). The TRC is considerably influenced by the rail pad stiffness when the train speed is less than 100 km/h (Figures 12(a) and 12(b)). As indicated in Figures 12(c) and 12(d), in the presence of CAM resilient layer, the TRC is increased considerably as the rail pad stiffness is increased (up to 70%) for all ranges of train speed.

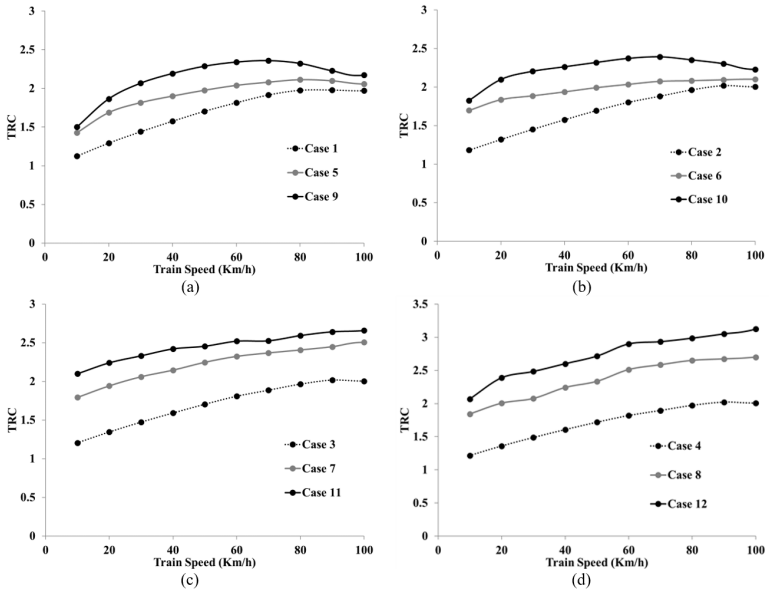

Figure 12 Variations of TRC versus train speed for random irregularities with high severity in various resilient layers: (a) PU-Soft; (b) PU-Hard; (c) CAM-Soft; (d) CAM- Hard.

Random irregularity with medium and low severity

Changes of the TRC against train speeds for random irregularities with medium and low severities in various types of rail pads and resilient layers are presented in Figures 13 and 14, respectively. The results indicate that as the severity of rail irregularity increases from low to medium, the level of TRC increases about 70 to 100 percent in different ranges of track flexibility. Moreover, the effect of track flexibility on the level of TRC increases when severity of rail irregularity increases. For instance, the maximum difference between the TRC obtained from the model when using CAM-Hard (case 5) and PU-Soft (case 8) is about 22%. This comparison was made when a soft rail pad was used, train speed was 100 km/h, and rail had irregularity with medium severity. The severity of the rail irregularities has substantial influence on the results such that if rail irregularity changes from medium to low, the difference decreases to 14%. However, when the rail pad stiffness changes from low (soft pad) to high (hard pad), the difference reaches to 36% in presence of irregularity with medium severity.

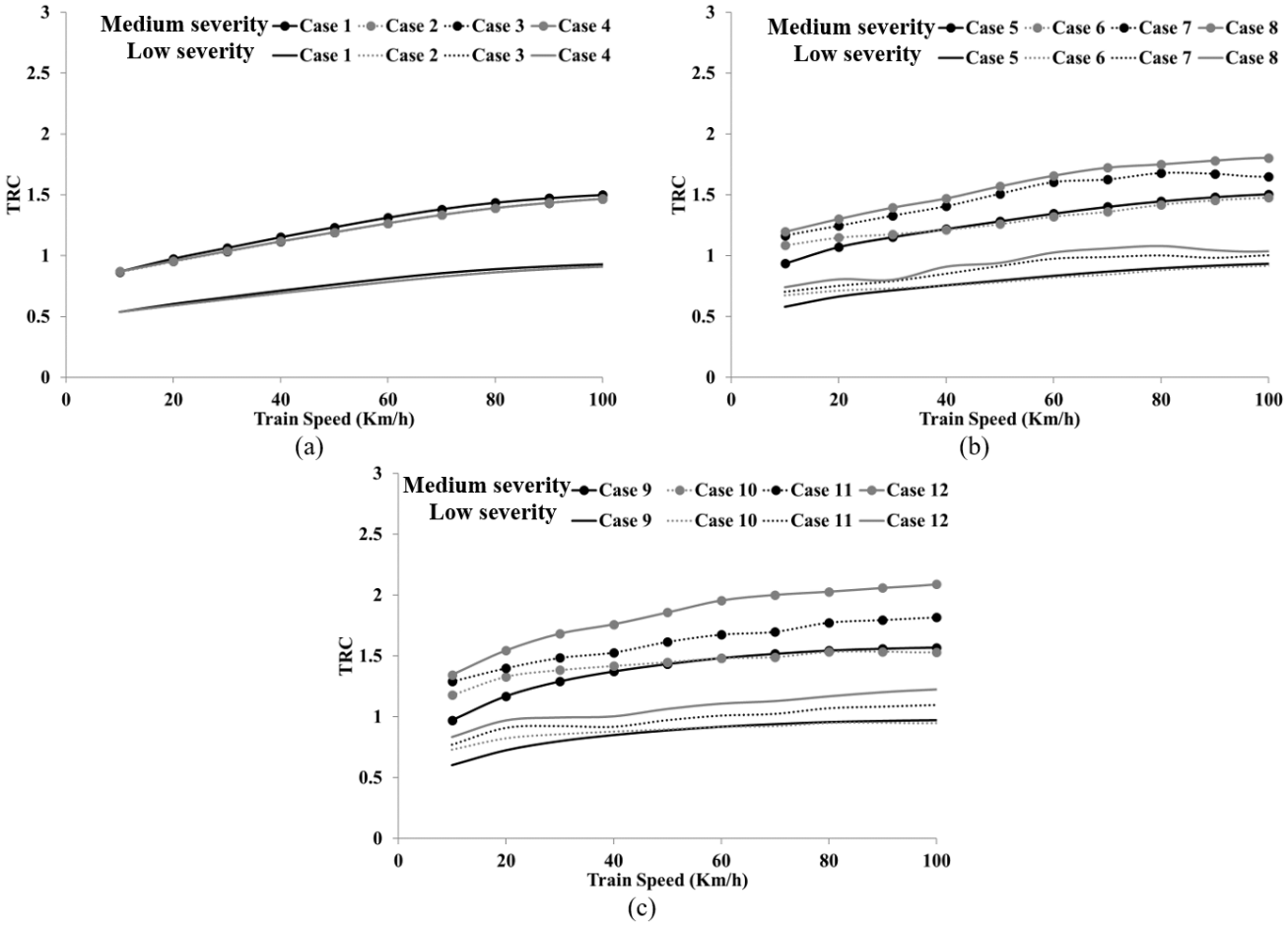

Figure 13 Variations of TRC versus train speed for random irregularities with medium and low severity in various rail pads: (a) Soft rail pad; (b) Medium rail pad; (c) Hard rail pad.

4.2 Effects of rolling stock parameters on the TRC

Damping and stiffness of vehicle suspension systems are the main parameters which have notable influences on the level of the TRC. They are presented by a factor called damping ratios of vehicle suspension systems. Damping ratios of primary and secondary suspension systems of a vehicle are defined as follows: (Dumitriu 2012, Dumitriu 2013, Dumitriu and Gheţi 2018, Dumitriu and Stănică 2019, Sadeghi et al. 2020)

$$DR_P = \frac{C_P}{\sqrt{K_P m_b}} \tag{12}$$

$$DR_S = \frac{C_S}{\sqrt{K_S m_C}} \tag{13}$$

DR_P stands for the damping ratio of primary suspension system, C_P and K_P are the damping and stiffness of primary suspension system and m_b stands for the mass of bogie. In equation (13), DR_S stands for the damping ratio of secondary suspension system, C_S and K_S are the damping and stiffness of secondary suspension system, and m_C stands for the mass of carbody (Dumitriu 2012, Dumitriu 2013, Dumitriu and Gheţi 2018, Dumitriu and Stănică 2019, Sadeghi et al. 2020).

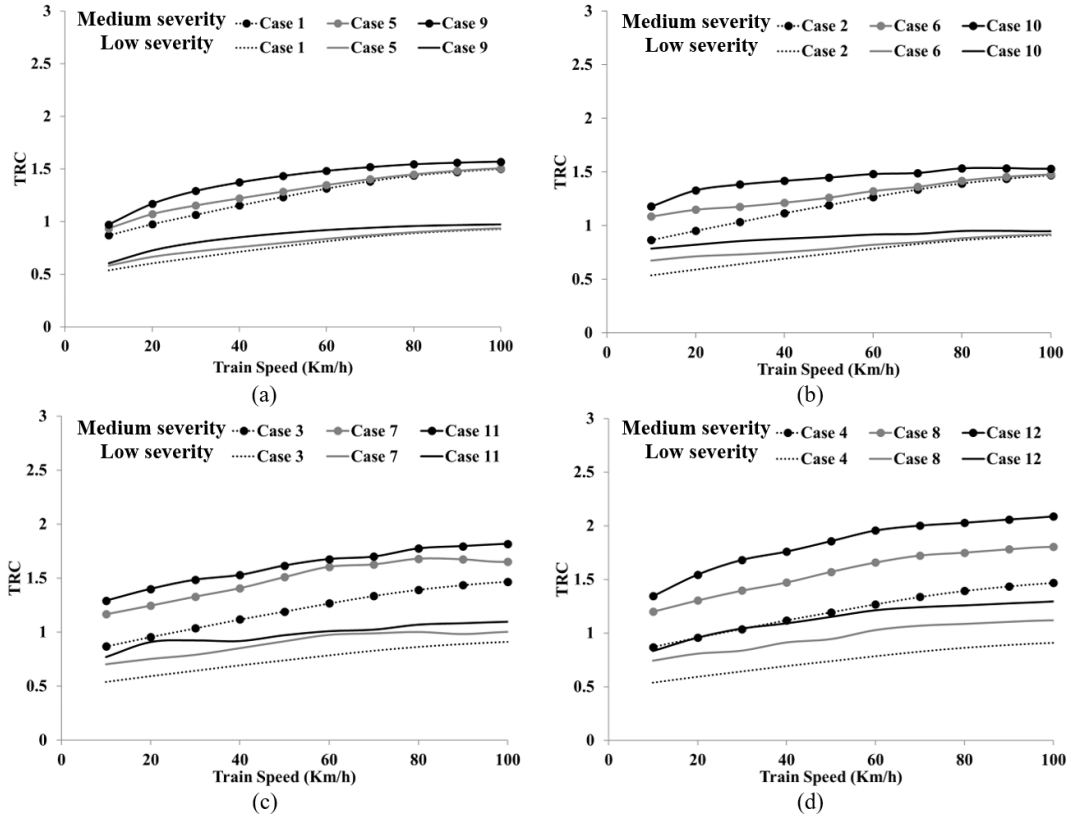

Figure 14 Variations of TRC versus train speed for random irregularities with medium and low severity in various resilient layers: (a) PU-Soft; (b) PU-Hard; (c) CAM-Soft; (d) CAM- Hard.

The effects of damping ratios on the TRC were investigated through a parametric study. For this purpose, the vehicle and slab-track properties were adopted from the CHR3 train and the CRTSII slab track, respectively. The effect of vehicle suspension systems on the TRC was studied for the train speeds of 50, 75 and 100 km/h, taking into consideration various amounts of track stiffness (Table 5).

The effects of various damping ratios of suspension systems on the TRC in different track stiffness and vehicle speeds are shown in Figures 15 to 17. Damping ratios of primary and secondary suspension systems of CHR3 railway vehicle are 1.23 and 0.67, respectively (Lei and Wang 2014).

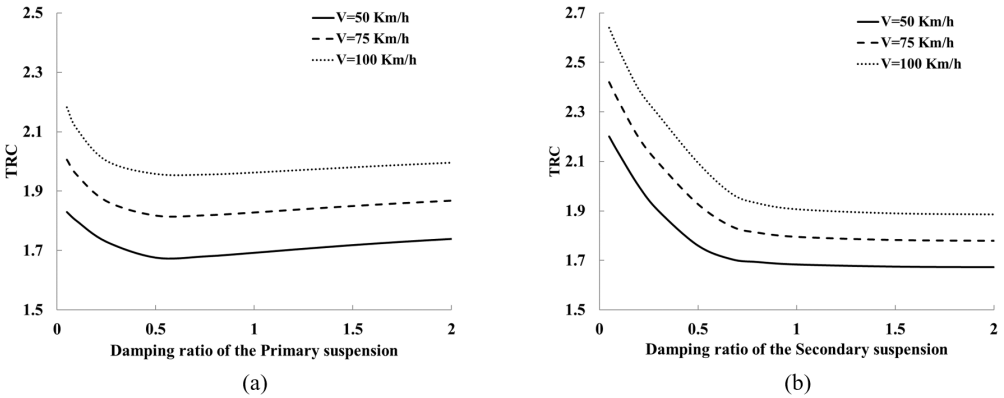

Figure 15 Variations of TRC versus damping ratio of various suspension systems in soft slab track: (a) primary suspension system; (b) secondary suspension system.

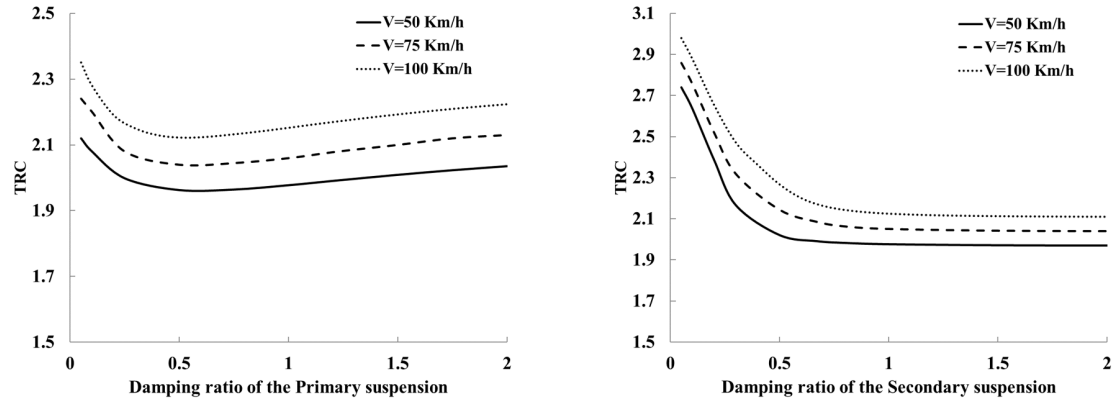

Figure 16 Variations of TRC versus damping ratio of various suspension systems in medium slab track: (a) primary suspension system; (b) secondary suspension system.

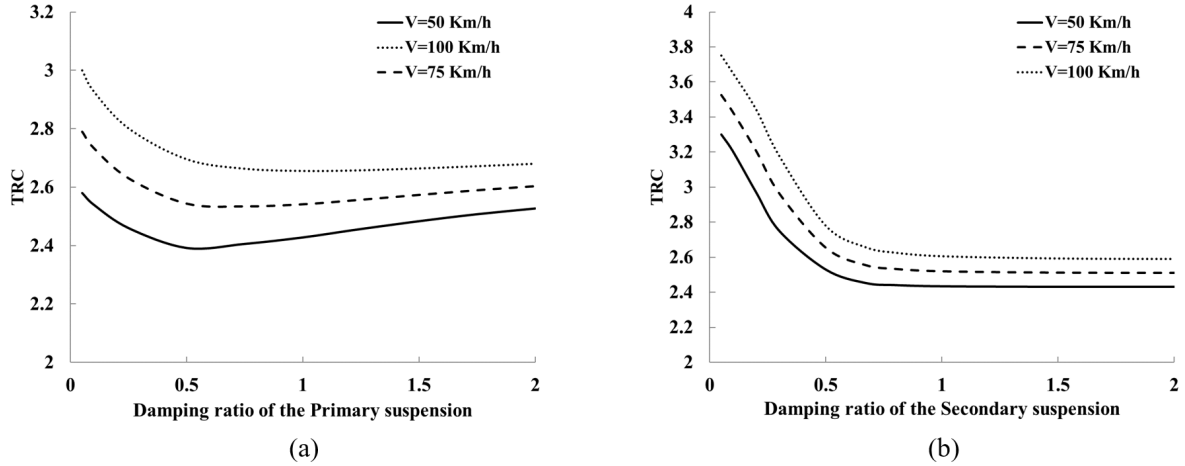

Figure 17 Variations of TRC versus damping ratio of various suspension systems in hard slab track: (a) primary suspension system; (b) secondary suspension system.

Table 5 characteristics of slab track with various stiffness in MN/m.

	Rail pad stiffness	Resilient layer stiffness
Soft slab track	15	5
Medium slab track	150	200
Hard slab track	500	900

Comparison of the results shows that damping ratio of secondary suspension system has a greater impact on the TRC. This is due to the fact that the bogie mass is between the primary suspension system and the carbody which reduces damping efficiency of primary suspension system (Dumitriu 2012, Dumitriu 2013, Dumitriu and Gheţi 2018, Dumitriu and Stănică 2019, Sadeghi et al. 2020). The changes in damping ratio of primary suspension can cause a maximum of 16% difference in the TRC. Variations in the damping ratio of secondary suspension system cause up to 45% change in the TRC. As the vehicle speed increases, the level of TRC increases. According to Figures 15 to 17, the pattern of the variation of the TRC against damping ratios is not changed by the changes in the vehicle speed. It means that this pattern is constant for all vehicle speeds.

5 TRC prediction model

As illustrated above, the TRC is dependent on properties of rolling stock properties and track parameters conditions. It is presented in a mathematical form in equation 14:

$$TRC = TC(K_{RP}, K_{RL}, V, \alpha_{Irr}) \times VC(DR_P, DR_S) \tag{14}$$

where TRC is the level of train ride comfort (based on Sperling index); TC (track coefficient) and VC (vehicle coefficient) represent the track parameter conditions and the rolling stock properties, respectively; TC is the track conditions function (i.e., rail pad stiffness, resilient layer stiffness, vehicle speed and rail irregularity); and VC is the rolling stock function (i.e., damping ratios of primary and secondary suspension systems of the vehicle).

5.1 Derivation of TC function

The data obtained from the parametric study were imported into the STATGRAPHICS (STATGRAPHICS Centurion 18 2020) in order to develop a mathematical expression for the TC (i.e., TRC as a function of track parameters properties). It was made in two steps. In the first step, the best possible mathematical relationship between the TRC and each variable (i.e., vehicle speed, rail pad stiffness, resilient layer stiffness and rail irregularity) was derived. It is indicated in equation (15) where P_j is the jth variable, $f_i(P_j)$ is the ith mathematical expression for the jth variable (P_j) and TRC_{ij} is the level of TRC for the ith mathematical expression of the jth variable. j was considered 1, 2, 3 and 4 for vehicle speed, rail pad stiffness, resilient layer stiffness and rail irregularity, respectively.

$$TRC_{ij} = f_i(P_j) \tag{15}$$

27 linear and nonlinear mathematical expressions (in forms of squared, exponential, polynomial with different order, multiplicative, logarithmic, and power) were considered. In other word, i changes from 1 to 27 in equation (15). The mathematical expression ($f_{best}(P_j)$) with the maximum R-squared (minimum error) was selected between each input parameters and output parameter. In the second step, the obtained mathematical models ($f_{best}(P_1)$, $f_{best}(P_2)$, $f_{best}(P_3)$, $f_{best}(P_4)$) were combined to form the function of track properties (TC). In this regard, 30 forms of combination were used to derive the most accurate expression (i.e., with the maximum R-squared: minimum error) for the TRC (as a function of all track parameters). It is presented under:

$$TC = \alpha_{Irr}\left[\frac{\exp(-0.03+0.2\ln(V))+(1.4+0.01\sqrt{K_{RP}})^2+\sqrt{(5+0.035\sqrt{K_{RL}})}}{3}\right] \tag{16}$$

$$\alpha_{Irr} = \begin{cases} \alpha_1 = 1 & Irregularities\ with\ high\ amplitude \\ \alpha_2 = 0.68 & Irregularities\ with\ medium\ amplitude \\ \alpha_3 = 0.42 & Irregularities\ with\ low\ amplitude \end{cases}$$

where α_{Irr} is the irregularity factor, K_{RP} is the rail pad stiffness in MN/m, K_{RL} is the resilient layer stiffness in MN/m and V is the vehicle speed in km/h.

5.2 Derivation of VC function

The effects of rolling stock properties on the TRC (obtained from the parametric study) were used to derive a relationship between vehicle properties and the TRC. As shown in Figures 15 to 17, the pattern of the variation of TRC against damping ratios of vehicle suspension systems is the same for all train speeds. Therefore, vehicle speed is considered constant in the derivation of the vehicle function (VC). For this purpose, the percentages of decrease or increase in damping ratio of suspension systems against variation percentages of the TRC were calculated (for the vehicle speed of 100 km/h). The results are presented in Figure 18 where the values in the horizontal axes in Figures 18(a) and 18(b) were obtained from $\left(\left(\frac{DR_P}{1.23}\right)-1\right)\times 100$ and $\left(\left(\frac{DR_S}{0.67}\right)-1\right)\times 100$, respectively (Sadeghi et al. 2020).

The level of TRC is 2.17 for the speed of 100 km/h (refer to Figure 11), therefore the values in the vertical axes were obtained from $\left(\left(\frac{TRC}{2.17}\right)-1\right)\times 100$. Polynomial expressions with order of 3 and 4 were used to make the best fit for the data presented in Figure 18. The best fit was used to compute the vehicle coefficient for other types of railway vehicles. This was led to an equation for the vehicle function (VC) (Sadeghi et al. 2020). Subsequently, the factors of primary and secondary suspension systems were obtained as follows:

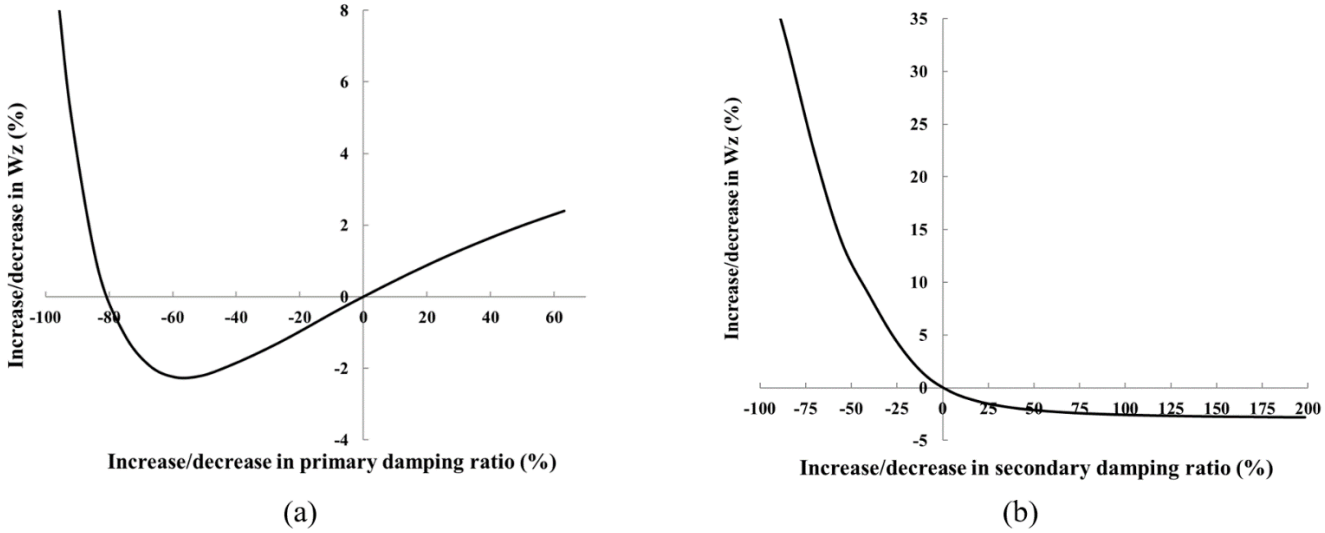

Figure 18 Percentage variations of W_Z versus the percentage of increase/decrease in damping ratio of various suspension systems in vehicle speed of 100 km/h: (a) primary suspension system; (b) secondary suspension system.

$$F_p = \left(3 \times 10^{-11}\emptyset_p{}^6 + 1 \times 10^{-10}\emptyset_p{}^5 - 1 \times 10^{-7}\emptyset_p{}^4 - 3 \times 10^{-6}\emptyset_p{}^3 + 0.0001\emptyset_p{}^2 + 0.0484\emptyset_p - 0.0633\right)/100 \quad (17)$$

$$F_S = \left(-9 \times 10^{-13}\emptyset_s{}^6 + 2 \times 10^{-10}\emptyset_s{}^5 + 2 \times 10^{-8}\emptyset_s{}^4 - 1 \times 10^{-5}\emptyset_s{}^3 + 0.0019\emptyset_s{}^2 - 0.1074\emptyset_s + 0.073\right)/100 \quad (18)$$

where, ϕ_P and ϕ_S stand for the percentage of decrease or increase in the damping ratio of primary and secondary suspension systems, respectively; and F_p and F_S are the functions related to primary and secondary suspension systems, respectively. Based on damping ratios of primary and secondary suspension systems of the CHR3 vehicle, equations (19) and (20) were derived: (Sadeghi et al. 2020)

$$\phi_P = \left(1 - \left(\frac{DR_P}{1.23}\right)\right) \times 100 \quad (19)$$

$$\phi_S = \left(1 - \left(\frac{DR_S}{0.67}\right)\right) \times 100 \quad (20)$$

In which DR_P and DR_S are the damping ratios of primary and secondary suspension systems of railway vehicles. Finally, the vehicle function (VC) was obtained as follows:

$$VC = (1 + F_p) \times (1 + F_S) \quad (21)$$

6 Application of prediction model

An algorithm for computation of ride comfort index based on propperties of track and rolling stock parameters is presented in Figure 19. In order to investigate reliability of the prediction model, application of the model in practice (i.e., in a railway field) was illustrated.

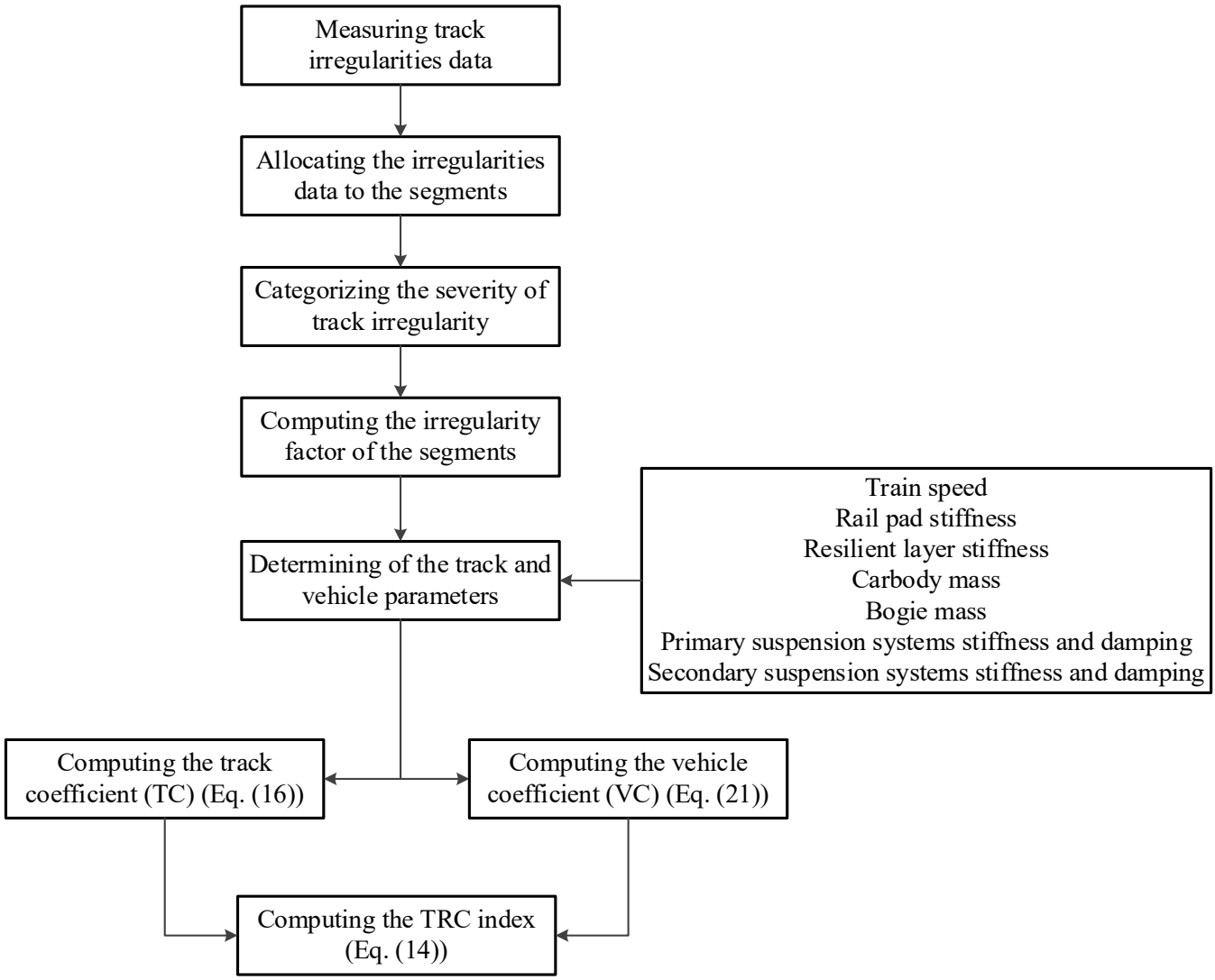

Figure 19 Algorithm of the TRC prediction model.

To this end, two types of slab track with various ranges of track flexibility and different severities of rail irregularity were selected in railway fields. The TRC were obtained from field measuremts. The results obtained from the measusremets were compared with those predicted by the model. The first location of the test was between Beheshti and Mosalla stations in Tehran's subway network (the oldest subway network in Iran) (Figure 20(a)). The second test was carried out in Isfahan Metro (Figure 20(b)). The superstructure of the slab track in Tehran field test consists of three layers: rail, concrete slab and the tunnel lining (concrete base). There is a cement asphalt mortar layer (CAM) between the concrete slab and the tunnel lining which forms a direct fixation fastening (DFF) (Figure 21(a)). The location of the test prefomed in Isfahan metro is adjacent to several monumental buildings. It has a super-soft superstructure constructed under the rails called Floating slab Track with High Resilient Fastener (FST-HRF) (Figure 21(c)). Schematic views of the two types of field tests are shown in Figure 21. The properties of slab track of Isfahan metro is presented in Table 1. The properties of slab track in Tehran metro are available in Sadeghi et al. (2016b). Physical and geometry properties of the train used in the Isfahan field test are presented in Table 2. Specifications of the train used in the Tehran field test are available in CNR CR (2002). The entire route of the test line in Tehran's metro with the length of 1 km was divided into 25 segments, each having a length of 40 meters. The slab-track in Isfahan's metro consists of FST-HRF, having a length of 0.4 km (Km 12+352 to 12+752). They were divided into 10 segments. Rail irregularities were measured by an EM-50 recording machine and a trolley system. The rail irregularity profiles measured for each track segment in Tehran and Isfahan's metro are presented in Figure 22. The tests were performed with train speeds of 30 and 50 km/h.

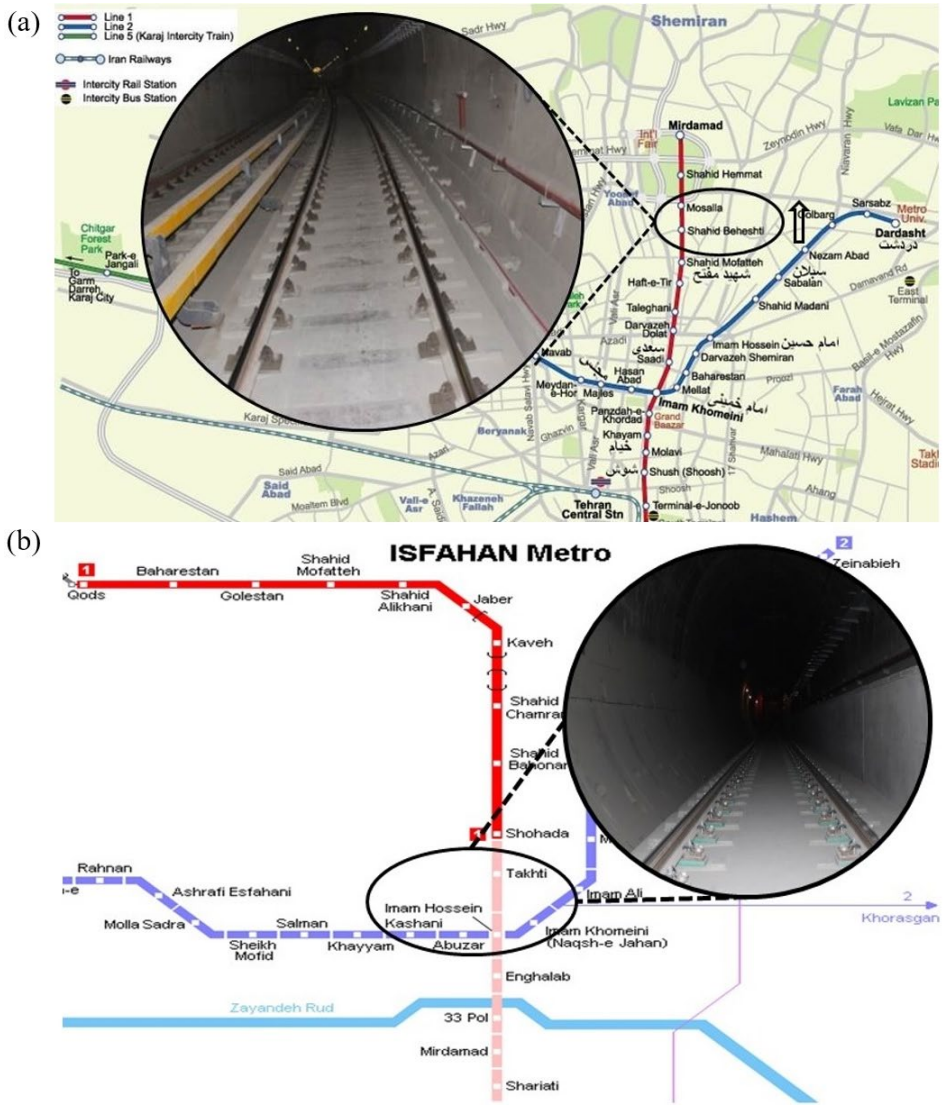

Figure 20 Field test locations: (a) in Tehran metro line 1 between Shahid Beheshti and Mosalla stations; (b) in Isfahan metro line 1 between Takhti and Imam Hossein stations.

Based on Figure 22(b), the maximum amplitude of rail irregularity of Isfahan field is 0.6 mm, so it is categorized as an irregularity with low severity. The maximum irregularity amplitude of Tehran field test is 3 mm (see Figure 22(a)) which is an irregularity with medium severity. The maximum irregularity amplitudes in the Tehran and Isfahan filed tests were obtained in the 11^{th} and 9^{th} segments (See Figure 22), respectively. The input parameters of TRC prediction model are listed in Table 6. The results obtained from the TRC prediction model and those of the field tests for various train speeds are presented in Table 7.

Table 6 The input parameter of TRC prediction model.

Test location	Tehran metro	Isfahan metro
Track type	DFF	FST-HRF
Severity of irregularity	medium	low
Rail pad stiffness (MN/m)	120	15.6
Resilient layer stiffness (MN/m)	900	14.5
Vehicle speed (km/h)	30, 50	30, 50
Bogie mass (kg)	7470	5300
Vehicle primary suspension stiffness (KN/m)	931.95	970
Carbody mass (kg)	22000	21400
Vehicle secondary suspension stiffness (KN/m)	347.5	275

As indicated in Table 7, the differences for the TRC obtained in the measurements and those of the prediction model are in the range of 7.5% to 16%. According to Table 7, the level of TRC estimated by the model is approximately higher than those measured in the field test. Comparison of the results indicates that the results of TRC prediction model are in relatively good agreement. The model predictions are more accurate for the tracks (segments) with more irregularity amplitudes.

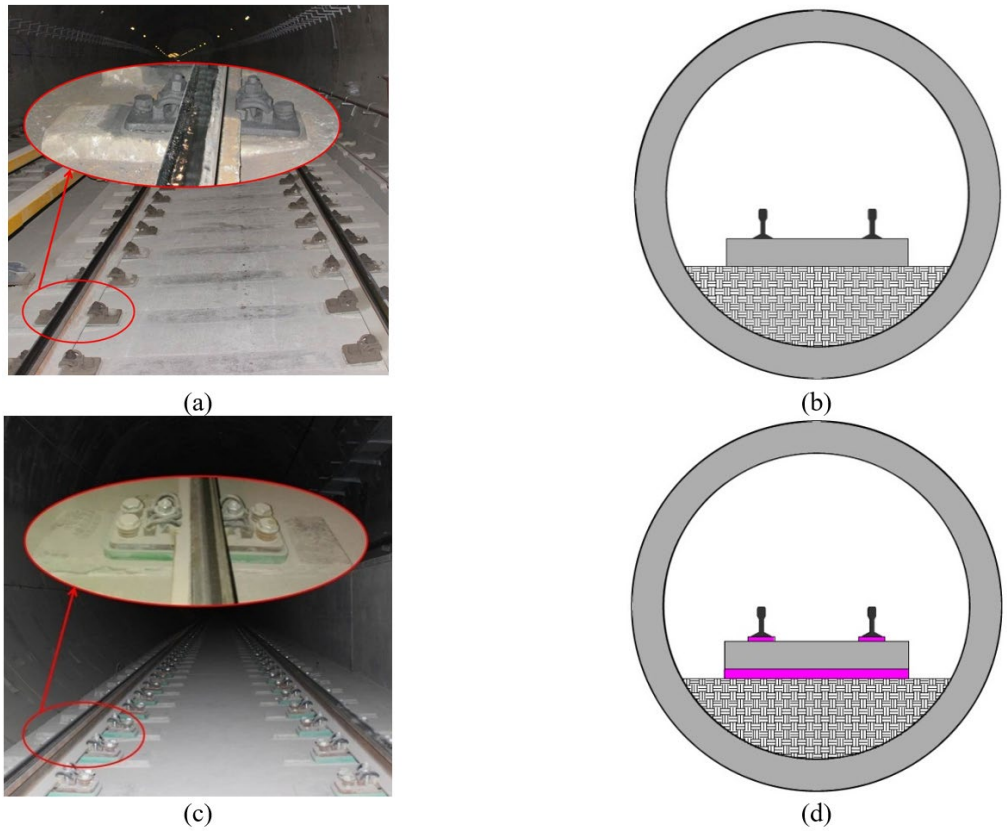

Figure 21 Views of the various superstructures of slab-track in the field tests: (a) Direct fixation fastening (DFF) (Tehran's metro); (b) A schematic views of DFF; (c) Floating slab Track with High Resilient Fastener (FST-HRF) (Isfahan's metro); (d) A schematic views of FST-HRF.

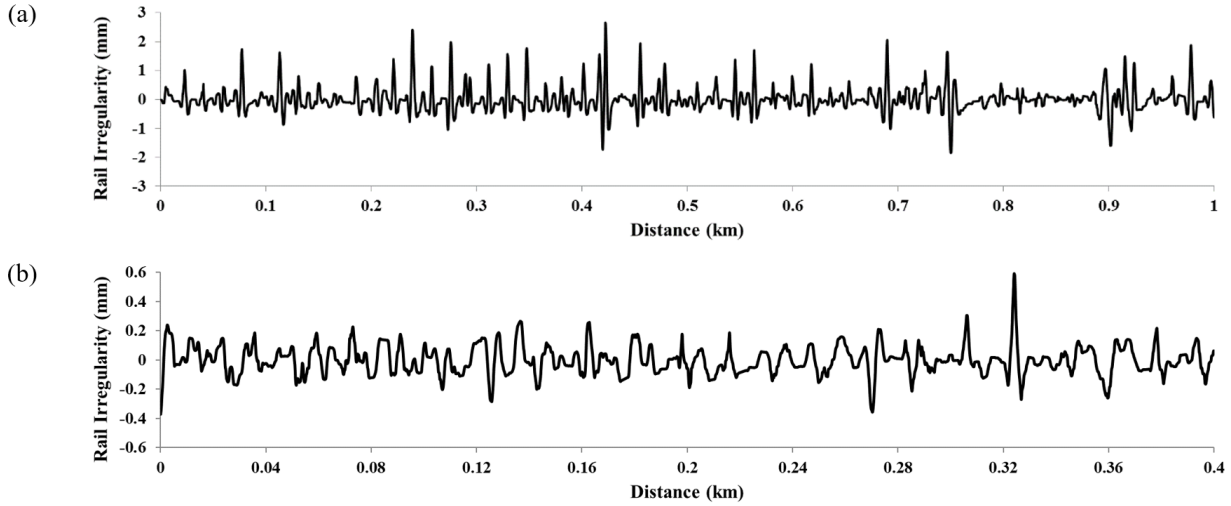

Figure 22 Rail irregularity of field test location: (a) Tehran's metro (b) Isfahan's metro.

The results show that the model developed in this study is a low-cost tool to estimate the level of TRC. It is very helpful to estimate the level of TRC (from track and rolling stock conditions) for making decisions on railway operation restrictions and track maintenance required actions.

Table 7 Comparison between results of TRC prediction model and field measurements in segment with the maximum amplitude.

Speed (km/h)	Tehran metro		Isfahan metro	
	field test	prediction model	field test	prediction model
30	1.44	1.67	0.85	0.98
50	1.58	1.72	0.95	1.02

7 Conclusions

Although Train Ride Comfort (TRC) is one of the most important vibration indicator of railway vehicle performance, there is no trace of TRC prediction model for the slab tracks in the literature. In response to this need, a TRC prediction model was developed in this research, taking into account all the track and rolling stock influencing parameters. To this end, a vehicle/track interaction model was developed. The validity of the model was shown through a comparison between results obtained from the model and those of a field test carried out in this research. The influences of track parameters and vehicle properties on the level of TRC were investigated through a two-phased parametric study.

The effects of rail-pad stiffness, resilient layer stiffness, subgrade stiffness and rail irregularity on the level of TRC in presence of various vehicle speeds were investigated in the first phase of the parametric study. The results indicate that although subgrade stiffness has not significant influence on the TRC, rail pad stiffness and resilient layer stiffness are effective parameters on the TRC. The level of TRC is not influenced by the resilient layer stiffness when the rail pad is soft. As the rail pad stiffness is increased, the influence of resilient layer stiffness on the TRC is increased. As the severity of rail irregularity increases, the effect of track flexibility increases.

The effects of vehicle suspension properties on the level of TRC were investigated in the second phase of the parametric study. The results obtained from the parametric study show that damping ratio of secondary suspension system has a greater impact on the TRC when compared with that of primary suspension system. The possible changes in damping ratio of primary and secondary suspension systems can cause a maximum of 16% and 45% changes in the level of TRC, respectively. As the vehicle speed increases, the rate of the changes increases. The patterns of the variation of TRC against the damping ratio of various suspension systems for all vehicle speed are the same.

A TRC prediction model for railway slab track systems was developed based on the results obtained from the parametric study. The TRC prediction model was presented as a function of track parameters and vehicle characteristics. Reliability of the TRC prediction model was investigated through comparison between the results obtained from the prediction model and those of a comprehensive field test carried out in this study. This was made in presence of various track flexibilities and rail irregularity severities. It was shown that the TRC prediction model developed here is a reliable tool for estimation of the TRC from slab track properties, rolling stock parameters and track irregularities. The prediction model developed in this study can be used as an accurate and low-cost tool to estimate the level of TRC in the track design, operation and maintenance.

Author's Contributions: **Conceptualization,** J Sadeghi and S Rabiee; **Methodology,** S Rabiee and A Khajehdezfuly; **Investigation,** S Rabiee and A Khajehdezfuly; **Software,** S Rabiee and A Khajehdezfuly; **Validation,** S Rabiee and A Khajehdezfuly; **Writing - original draft,** S Rabiee and A Khajehdezfuly; **Writing - review & editing,** J Sadeghi; **Funding acquisition,** J Sadeghi and S Rabiee; **Resources,** S Rabiee, J Sadeghi and A Khajehdezfuly; **Supervision,** J Sadeghi.

Editor: Marcílio Alves.

References

Askarinejad, H., Dhanasekar, M. (2016). A multi-body dynamic model for analysis of localized track responses in vicinity of rail discontinuities. International Journal of Structural Stability and Dynamics 16(09): 1550058.

Au, F. T. K., Wang, J. J., Cheung, Y. K. (2002). Impact study of cable-stayed railway bridges with random rail irregularities. Engineering Structures 24(5): 529-541.

BS 6841. (1987). British Standard: Measurement and evaluation of human exposure to whole-body mechanical vibration and repeated shock.

Cheli, F., Corradi, R. (2011). On rail vehicle vibrations induced by track unevenness: Analysis of the excitation mechanism. Journal of Sound and Vibration 330(15): 3744-3765.

Cheng, Y. C., Hsu, C. T. (2014). Running safety and comfort analysis of railway vehicles moving on curved tracks. International Journal of Structural Stability and Dynamics 14(04): 1450004.

Cheng, Y. C., Hsu, C. T. (2016). Parametric analysis of ride comfort for tilting railway vehicles running on irregular curved tracks. International Journal of Structural Stability and Dynamics 16(09): 1550056.

Choi, I. I. Y., Um, J. H., Lee, J. S., Choi, H. H. (2013). The influence of track irregularities on the running behavior of high-speed trains. Proceedings of the Institution of Mechanical Engineers, Part F: Journal of rail and rapid transit 227(1): 94-102.

CNR CR. Car manuals for Tehran subway Line 1. Changchun Railway vehicles Co, China. (2002) Report No 2.

CNR CR. General description of train system, Isfahan metro project Line 1. Changchun Railway vehicles Co, China. (2014) Report No 2.

Connolly, D. P., Kouroussis, G., Laghrouche, O., Ho, C. L., Forde, M. C. (2015). Benchmarking railway vibrations–Track, vehicle, ground and building effects. Construction and Building Materials 92: 64-81.

Costa, P. A., Calçada, R., Cardoso, A. S. (2012). Influence of train dynamic modelling strategy on the prediction of track–ground vibrations induced by railway traffic. Proceedings of the Institution of Mechanical Engineers, Part F: Journal of Rail and Rapid Transit 226(4): 434-450.

Costa, P. A., Colaço, A., Calçada, R., Cardoso, A. S. (2015). Critical speed of railway tracks. Detailed and simplified approaches. Transportation Geotechnics 2: 30-46.

Dumitriu, M. (2012). Influence of the suspension damping on ride comfort of passenger railway vehicles. UPB Scientific Bulletin, Series D: Mechanical Engineering 74(4): 75-90.

Dumitriu, M. (2013). Evaluation of the comfort index in railway vehicles depending on the vertical suspension features. Annals of the Faculty of Engineering Hunedoara 11(4): 23.

Dumitriu, M., Gheţi, M. A. (2018, November). Numerical study on the influence of primary suspension damping upon the dynamic behaviour of railway vehicles. In IOP Conference Series: Materials Science and Engineering, IOP Publishing Vol. 444, No. 4, 042001.

Dumitriu, M., Stănică, D. I. (2019). Influence of the Primary Suspension Damping on the Ride Comfort in the Railway Vehicles. In Materials Science Forum, Trans Tech Publications Ltd Vol. 957, 53-62.

EN 12299. (2009). European Committee for Standardization: Railway applications—Ride comfort for passengers—Measurement and evaluation.

Esveld, C. (1989). Modern railway track. MRT-productions.

Fernández Ruiz, J., Costa, P. A., Calçada, R., Medina Rodríguez, L. E., Colaço, A. (2017). Study of ground vibrations induced by railway traffic in a 3D FEM model formulated in the time domain: experimental validation. Structure and Infrastructure Engineering 13(5): 652-664.

Garg, V. K., Dukkipati, R. V. (1984), Dynamics of Railway Vehicle Systems, Academic Press.

Graa, M., Nejlaoui, M., Houidi, A., Affi, Z., Romdhane, L. (2014). Modeling and simulation for vertical rail vehicle dynamic vibration with comfort evaluation. In Conference on Multiphysics Modelling and Simulation for Systems Design (pp. 47-57).

IMER Co. (2005). Superstructure of Isfahan's metro, Report No.2.

ISO 2631-1. (1997). International Organization for Standardization: Mechanical vibration and shock — Evaluation of human exposure to whole–body vibration — Part 1: General requirements.

Iwnicki, S. (2006). Handbook of railway vehicle dynamics. CRC Press.

Kargarnovin, M. H., Younesian, D., Thompson, D., Jones, C. (2005). Ride comfort of high-speed trains travelling over railway bridges. Vehicle System Dynamics 43(3): 173-197.

Ketchum, C. D., Wilson, N. (2012). Performance-Based Track Geometry, Phase 1 (No. TCRP Project D-7, Task 18).

Khajehdezfuly, A. (2019). Effect of rail pad stiffness on the wheel/rail force intensity in a railway slab track with short-wave irregularity. Proceedings of the Institution of Mechanical Engineers, Part F: Journal of Rail and Rapid Transit 233(10): 1038-1049.

Kim, Y. G., Kwon, H. B., Kim, S. W., Kim, C. K., Kim, T. W. (2003). Correlation of ride comfort evaluation methods for railway vehicles. Proceedings of the Institution of Mechanical Engineers, Part F: Journal of Rail and Rapid Transit 217(2): 73–88.

Kim, Y. S., Lim, T. K., Park, S. H., Jeong, R. G. (2008). Dynamic model for ride comfort evaluations of the rubber-tired light rail vehicle. Vehicle System Dynamics 46(11): 1061-1082.

Kouroussis, G., Connolly, D. P., Verlinden, O. (2014). Railway-induced ground vibrations–a review of vehicle effects. International Journal of Rail Transportation 2(2): 69-110.

Kouroussis, G., Verlinden, O., Conti, C. J. V. S. D. (2012). Influence of some vehicle and track parameters on the environmental vibrations induced by railway traffic. Vehicle system dynamics 50(4): 619-639.

Kumar, V., Rastogi, V., Pathak, P. M. (2017). Simulation for whole-body vibration to assess ride comfort of a low–medium speed railway vehicle. Simulation 93(3): 225-236.

Lei, X. (2017). High speed railway track dynamics. Models, Algorithms and Applications. Science Press, Beijing/Springer Nature Singapore Pte. Ltd.

Lei, X., Wang, J. (2014). Dynamic analysis of the train and slab track coupling system with finite elements in a moving frame of reference. Journal of Vibration and Control 20(9): 1301-1317.

Lei, X., Zhang, B. (2010). Analysis of dynamic behavior for slab track of high-speed railway based on vehicle and track elements. Journal of Transportation Engineering 137(4): 227-240.

Ling, L., Zhang, Q., Xiao, X., Wen, Z., Jin, X. (2018). Integration of car-body flexibility into train–track coupling system dynamics analysis. Vehicle System Dynamics 56(4): 485-505.

Mosayebi, S. A., Esmaeili, M., Zakeri, J. A. (2017). Numerical investigation of the effects of unsupported railway sleepers on train-induced environmental vibrations. Journal of Low Frequency Noise, Vibration and Active Control 36(2): 160-176.

Mosayebi, S. A., Esmaeili, M., Zakeri, J. A. (2020). Dynamic Train–Track Interactions and Stress Distribution Patterns in Ballasted Track Layers. Journal of Transportation Engineering, Part B: Pavements 146(1): 04019042.

Sadeghi, J., Esmaeili, M. H. (2018) Effectiveness of track stiffness reduction in attenuation of metro induced vibrations received by historical buildings, Latin American Journal of Solids and Structures 15(11): 1-11.

Sadeghi, J., Khajehdezfuly, A., Esmaeili, M., Poorveis, D. (2016a). An efficient algorithm for nonlinear analysis of vehicle/track interaction problems. International Journal of Structural Stability and Dynamics 16(08): 1550040.

Sadeghi, J., Khajehdezfuly, A., Esmaeili, M., Poorveis, D. (2016b). Investigation of rail irregularity effects on wheel/rail dynamic force in slab track: comparison of two and three dimensional models. Journal of Sound and Vibration 374: 228-244.

Sadeghi, J., Khajehdezfuly, A., Heydari, H., Askarinejad, H. (2020). Development of Railway Ride Comfort Prediction Model: Incorporating Track Geometry and Rolling Stock Conditions. Journal of Transportation Engineering, Part A: Systems 146(3): 04020006.

Sadeghi, J., Rabiee, S., Khajehdezfuly, A. (2019). Effect of rail irregularities on ride comfort of train moving over ballast-less tracks. International Journal of Structural Stability and Dynamics 19(06): 1950060.

STATGRAPHICS Centurion 18 (2020). Statistical analysis software (version 18), http://www.statgraphics.com

Sun, Y. Q., Dhanasekar, M. (2002). A dynamic model for the vertical interaction of the rail track and wagon system. International Journal of Solids and Structures 39(5): 1337-1359.

UIC 513R. (1994). International Union of Railways: Guidelines for evaluating passenger comfort in relation to vibration in railway vehicle.

Van Eldik Thieme, I. H. (1961). Passenger riding comfort criteria and methods of analysing ride and vibration data (No. 610173). SAE Technical Paper.

Wei, K., Zhang, P., Wang, P., Xiao, J., Luo, Z. (2016). The influence of amplitude-and frequency-dependent stiffness of rail pads on the random vibration of a vehicle-track coupled system. Shock and Vibration.

Wu, Y. S., Yang, Y. B. (2003). Steady-state response and riding comfort of trains moving over a series of simply supported bridges. Engineering Structures 25(2): 251-265.

Xu, J., Wang, B., Wang, L., Wang, P. (2016). Distribution characteristics and influencing factors of the frequency-domain response of a vehicle–track vertical coupled system. Journal of Modern Transportation 24(3): 166-176.

Yang, Y. B., Yau, J. D., Yao, Z., Wu, Y. S. (2004). Vehicle-bridge interaction dynamics: with applications to high-speed railways. World Scientific.

Yau, J. D., Yang, Y. B., Kuo, S. R. (1999). Impact response of high speed rail bridges and riding comfort of rail cars. Engineering Structures 21(9): 836-844.

Youcef, K., Sabiha, T., El Mostafa, D., Ali, D., Bachir, M. (2013). Dynamic analysis of train-bridge system and riding comfort of trains with rail irregularities. Journal of Mechanical Science and Technology 27(4): 951-962.

Zakeri, J. A., Esmaeili, M., Heydari-Noghabi, H. (2016). A field investigation into the effect of under sleeper pads on the reduction of railway-induced ground-borne vibrations. Proceedings of the Institution of Mechanical Engineers, Part F: Journal of Rail and Rapid Transit 230(3): 999-1005.

Zakeri, J. A., Feizi, M. M., Shadfar, M., Naeimi, M. (2017). Sensitivity analysis on dynamic response of railway vehicle and ride index over curved bridges. Proceedings of the Institution of Mechanical Engineers, Part K: Journal of Multi-Body Dynamics 231(1): 266-277.

Zhai, W., Liu, P., Lin, J., Wang, K. (2015). Experimental investigation on vibration behaviour of a CRH train at speed of 350 km/h. International Journal of Rail Transportation 3(1): 1-16.

Zhai, W., Wang, K., Cai, C. (2009). Fundamentals of vehicle–track coupled dynamics. Vehicle System Dynamics 47(11): 1349-1376.

Zhang, J., Gao, Q., Tan, S. J., Zhong, W. X. (2012). A precise integration method for solving coupled vehicle–track dynamics with nonlinear wheel–rail contact. Journal of Sound and Vibration 331(21): 4763-4773.

Zhang, J., Zhao, Y., Zhang, Y. H., Jin, X. S., Zhong, W. X., Williams, F. W., Kennedy, D. (2013). Non-stationary random vibration of a coupled vehicle–slab track system using a parallel algorithm based on the pseudo excitation method. Proceedings of the Institution of Mechanical Engineers, Part F: Journal of Rail and Rapid Transit 227(3): 203-216.